Nano Energy 85 (2021) 106012

Contents lists available at ScienceDirect

Nano Energy

journal homepage: http://www.elsevier.com/locate/nanoen

TENG-Bot: Triboelectric nanogenerator powered soft robot made of uni-directional dielectric elastomer

Wenjie Sun [a,1], Bo Li [b,1], Fei Zhang [a], Chunlong Fang [c], Yanjun Lu [a], Xing Gao [d], Chongjing Cao [d], Guimin Chen [b,*], Chi Zhang [c,*], Zhong Lin Wang [c,e,**]

[a] School of Mechanical and Precision Instrument Engineering, Xi'an University of Technology, Xi'an 710048, China
[b] State Key Laboratory for Manufacturing System Engineering, Shaanxi Key Lab for the intelligent Robots, School of Mechanical Engineering, Xi'an Jiaotong University, Xi'an 710049, China
[c] CAS Center for Excellence in Nanoscience, Beijing Key Laboratory of Micro-nano Energy and Sensor, Beijing Institute of Nanoenergy and Nanosystems, Chinese Academy of Sciences, Beijing 100083, China
[d] Research Centre for Medical Robotics and Minimally Invasive Surgical Devices, Shenzhen Institutes of Advanced Technology (SIAT), Chinese Academy of Sciences, Shenzhen 518055, China
[e] School of Materials Science and Engineering, Georgia Institute of Technology, Atlanta, GA 30332, USA

ARTICLE INFO

Keywords:
Conjunction system
Dielectric elastomer
Energy harvesting
Freestanding TENG
Soft robot

ABSTRACT

A soft robot employing dielectric elastomer actuators (DEAs) exhibits a flexible body and dexterity locomotion in unstructured environments. However, conventional power supplies required by DEAs pose an obstacle for small-scale robotic system. Triboelectric nanogenerator (TENG) is capable of harvesting kinetic energy from the environment to generate matching power for DEA. Yet, a TENG-driven, DEA-based robot is hindered due to the nonlinear and insufficient mechanical transmission in robotic motion. In this paper, we developed an uni-directional DEA-driven soft robot. It aligns the direction of DEA in extension with the robot motion to achieve high efficient energy conversion, yielding a maximum crawling velocity of 110 mm (2.2 body-length) /sec and a payload capacity of 40 g. Then a TENG-Bot, that is a TENG-soft robot conjunction system, is built using a freestanding TENG. With the benefit from the simple structure, and the high efficiency of the robot, the electrical energy generated by the TENG can directly drive the robot without additional control panels. Experiments demonstrate a linear relationship between the sliding speed of the TENG and the velocity of the soft robot, a direct control correspondence. The TENG-Bot offers a route for developing self-powered soft robots by harvesting the environment motion.

1. Introduction

Soft robots are developed by elegantly integrating soft actuators, compliant structures, and stretchable sensors [1–5]. They have been demonstrated with promising potentials in medical operations [6], underwater manipulations [7], and human assistance [8], etc. Dielectric elastomer actuators (DEAs) are an emerging class of soft actuators with advantages of fast response, high energy densities and large strains that resemble human muscles [9, 10-12]. Different types of soft robots driven by DEA have been reported capable of diverse performances, including wall-climbing [13], swimming [14-16], crawling [17-22], object-grabbing [23-25] and drone flight [26]. However, a voltage exceeding 1000 V is needed for activating DEA, which usually requires the robot to be tethered to an off-board power supply [27,28]. Although on-board power electronics have been developed with integrated power modules [15,29], the operation duration is limited to minutes, which significantly restricts the mobility endurance of DEA-driven soft robotic systems.

Triboelectric nanogenerator (TENG), capable of generating high open-circuit voltage for capacitive devices [30], can provide an alternative solution for powering DEAs. The TENG can convert mechanical energy to electrical energy by coupling triboelectrification and

* Corresponding authors.
** Corresponding author at: CAS Center for Excellence in Nanoscience, Beijing Key Laboratory of Micro-nano Energy and Sensor, Beijing Institute of Nanoenergy and Nanosystems, Chinese Academy of Sciences, Beijing 100083, China.
E-mail addresses: guimin.chen@xjtu.edu.cn (G. Chen), czhang@binn.cas.cn (C. Zhang), zlwang@gatech.edu (Z.L. Wang).
[1] These authors contributed equally to this work.

https://doi.org/10.1016/j.nanoen.2021.106012
Received 25 January 2021; Received in revised form 6 March 2021; Accepted 17 March 2021
Available online 23 March 2021
2211-2855/© 2021 Elsevier Ltd. All rights reserved.

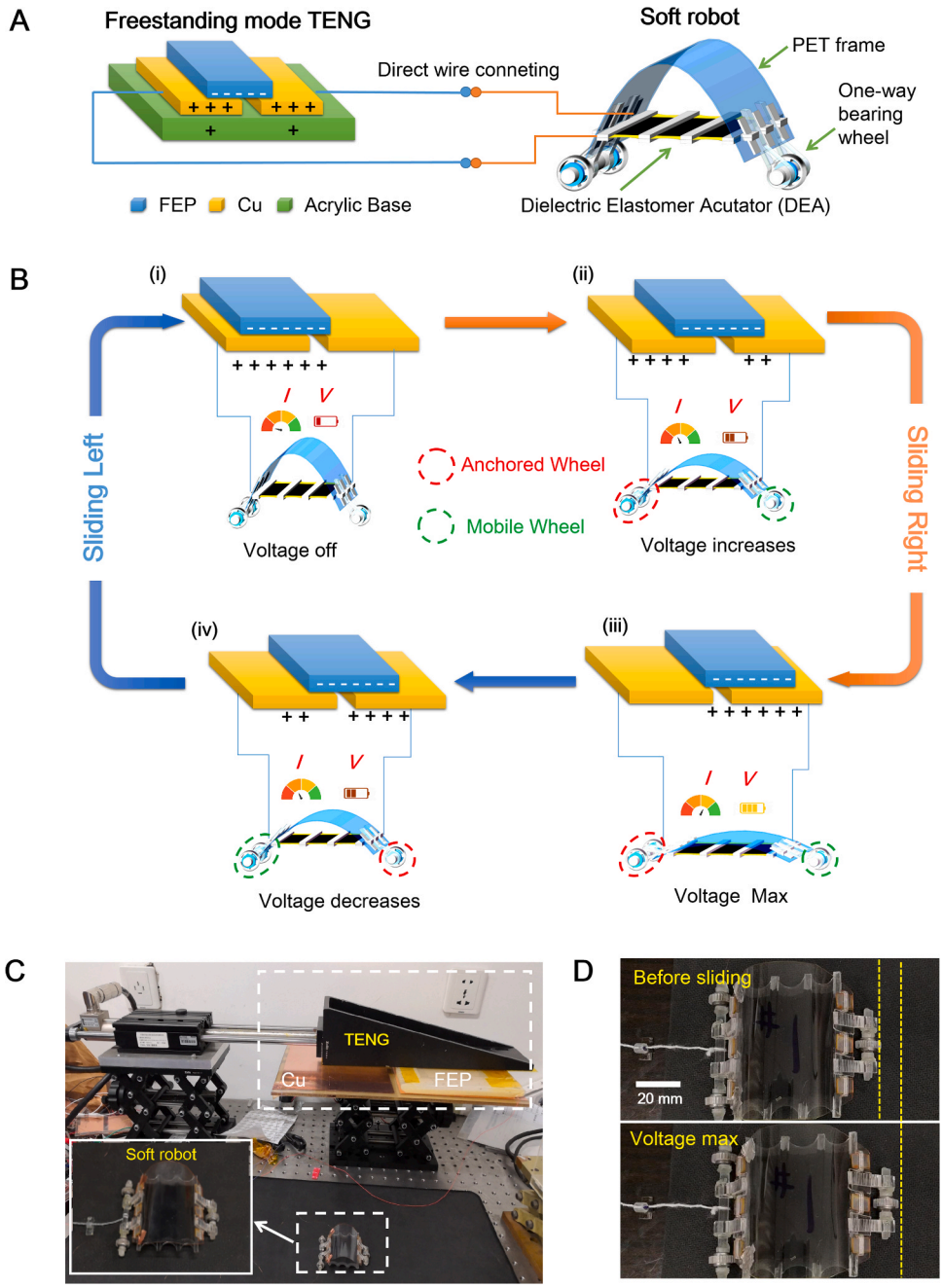

Fig. 1. The proposed TENG-Bot: TENG and soft robot conjunction system. (A) A freestanding TENG is directly connected to the soft robot. The soft robot is composed of a dielectric elastomer actuator (DEA), a compliant arc-shaped body and three one-way bearing wheels. **(B)** When sliding the TENG, a voltage is generated to actuate the DEA. The DEA elongates and retracts, producing a displacement of the robot. In one sliding cycle, the soft robot completes a locomotion step. **(C)** The conjunction system is established in the lab. **(D)** The power-off and power-max states of the soft robot, showing a forward displacement.

electrostatic induction [31-34], as a complementary power of the electromagnetic generator [35]. Literature has verified the TENG-actuated DEA as a self-powered optical modulator for tunable gating and transparency, where the static strain was regulated by TENG [36-39]. However, a kinetic motion of a DEA-based robot has not been realized. To our knowledge, this is because, in the previous soft robot design, the DEA has multi-DOF (degrees of freedom), but the soft robot may have only limited DOF in motion; so that the insufficient transmission has dissipated the majority of the energy, during the DEA strain being transmitted to robot displacement. This issue is less considered when the robot is powered by a conventional electromagnetic generator that provides sufficient energy. When a TENG power source is in conjunction with a soft robot, a higher efficient mechanical transmission shall be achieved considering a TENG can harvest limited energy.

In this paper, a TENG-Bot, soft robot that is suitable for TENG-powering and control, is proposed by utilizing an uni-directional DEA. The DEA eliminates electromechanical instability and outputs the strain in single DOF that in accordance with the direction of robot motion. Through the assembling of DEA and flexure robot body, the compliance gradient is established in a robot system, achieving a linear and real-time mechatronic robot system that TENG can direct power and control without additional control panel.

2. Results

2.1. The principle of TENG-soft robot conjunction system

Fig. 1(A) depicts the TENG-Bot as a TENG-soft robot conjunction system. A freestanding mode TENG is designed and connected to a soft robot. In the freestanding TENG, the moving component can slide freely on the fixed two substrates. Since the mobile layer is electrode free, it eliminates the electrostatic shield effect and leads to a high charge

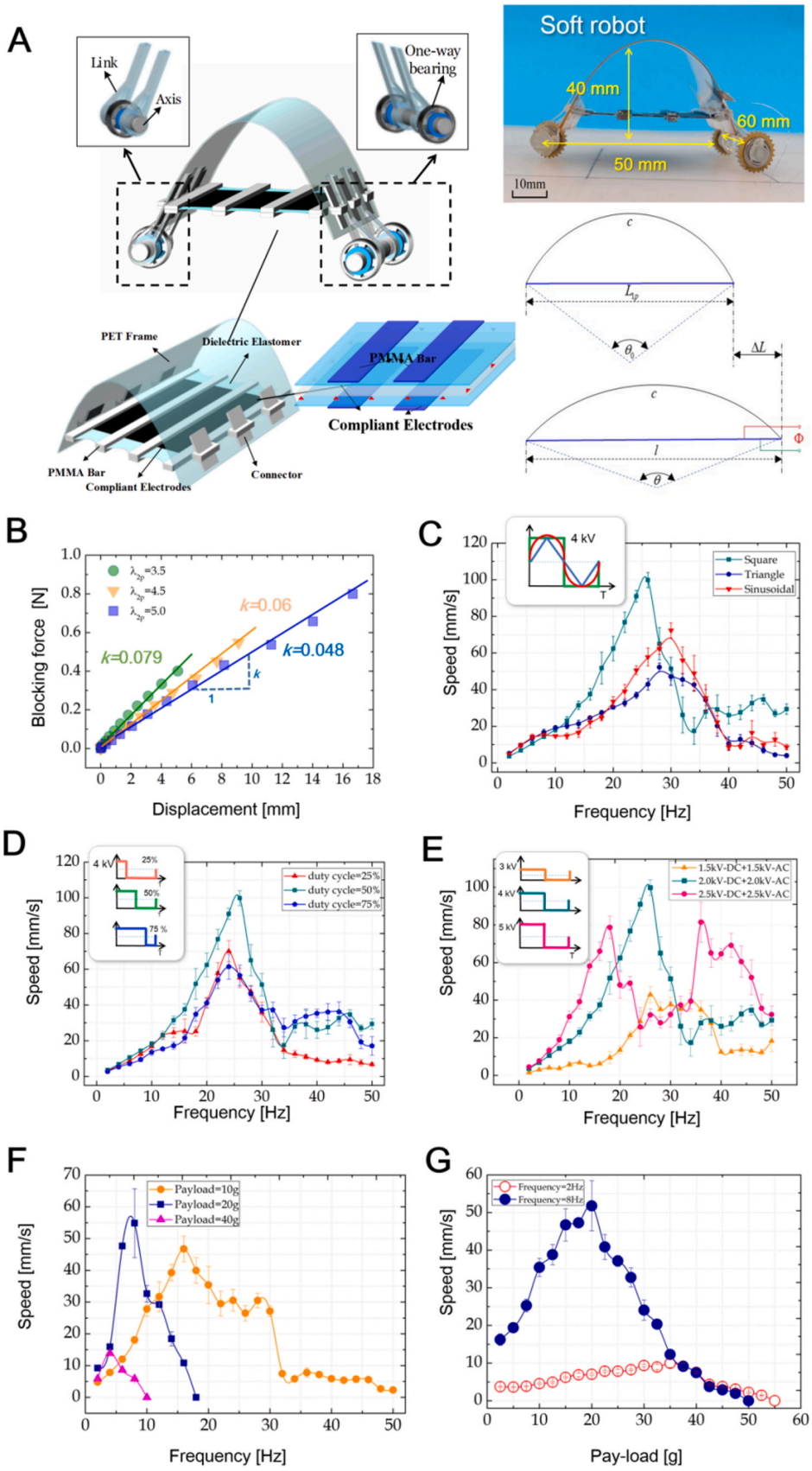

Fig. 2. Characterization of the soft robot. (A) The design of the soft robot with a uni-directional DEA. **(B)** The linear mechanical performance of the soft robot. **(C)** The relation between the speed of the robot and the voltage frequency with various voltage waveforms (square, triangle and sine waves). **(D)** The speed curve of the robot under different duty cycles. **(E)** The speed curve of the robot under different amplitude. **(F)** The speed of the soft robot as a function of the frequency. **(G)** The speed of the soft robot as a function of the weight of the payload.

transfer efficiency ~85% [39]. The generated high voltage is then applied to the soft robot through wires linked to the fixed substrate electrodes. The configuration of the freestanding mode reduces dynamic tethering constrains, since the moving part is not connect to the robot. The soft robot is composed of an uni-directional DEA, a PET flexible frame and three one-way bearing wheels. The DEA is a polymer capacitor, and its actuation voltage is related to the accumulated charges provided by the TENG. Unlike the previous soft robots with the DEAs integrated into the robot bodies, this robot features a modular design with robust mechanical assembling, hence achieving a highly desired linear actuation and motion performance.

Fig. 1(B) illustrates how the TENG powers the soft robot as a TENG-Bot: (i) At the beginning of the sliding, the TENG is at a neutral state, and the charge is not output. The soft robot is power off. (ii) When the TENG slides further to the right-hand side, electrical charges are accumulated on the DEA, which produces an increasing voltage, and the DEA elongates slightly. The one-way bearing wheels allow the soft robot to crawl, and the elongation in DEA is maintained by the anchored wheel. (iii) When the sliding is close to the boundary, the amount of charge is maximized that the voltage ramps to a maximum value. The DEA attains a maximum strain. (iv) When the TENG slides from the right end to the left-hand side, the voltage decreases, and the DEA retracts. Owing to the one-way bearings in the wheels, the forward displacement is maintained during the DEA contraction, and the soft robot crawls forward as a result.

Fig. 1(C) shows the conjunction system in the experiments. The TENG consists of three parts, a dielectric fluorinated ethylene propylene FEP thin film (25 μm) as a sliding part on two copper electrodes as the fixed parts that mounted on an acrylic substrate. For an improved output performance of the TENG, the downside surface of the FEP film was treated by inductive coupling plasma (ICP) to create nanorod structures [40]. In Fig. 1(D), the extension of the DEA during the robot crawling is illustrated.

2.2. Soft robot design and mechanical characterization

Fig. 2(A) describes the three-dimensional schematic view of the proposed soft robot, which composes of a piece of DEA, an arched PET frame, and connectors. As inspired by anchor-crawling of the inchworm [41], we use the wheels with one-way bearing as the feet of the soft robot. These components are assembled by rigid linkages. The so-obtained soft robot is of the dimensions of 50 mm × 60 mm× 40 mm and a weight of 10.5 g.

The specific preparation process of the DEA is described in the Supplementary Information (SI). In the pre-stretched state, due to the constraints of the flexible frame on the DE membrane, the DEA maintains uni-directional in-plane strain in the actuation direction. When a voltage is applied to the DE membrane, the DEA elongates in one direction, and it deploys of the arch body to reach a new equilibrium state, which is defined as the actuated state of the actuator (see Supplementary Movie S1). The design aligns the actuation direction and the motion direction of the robot, hence maximizing the energy efficiency to convert electrical energy to robot kinetics so that the TENG can benefit. Fig. 2(B) presents the relationship between the actuation stroke and the blocking force of the DEA in the robot body. Each data is under a prescribed voltage. In the static actuation, the elastic stress in DEA is always in equilibrium with the tensile force of the frame, so that the blocking force is expressed as $F_B = \frac{\varepsilon\Phi^2}{H^2}\lambda_{1p}^2\lambda_{2p}^2 \times \frac{Vol}{L_{1p}}$, (see detailed theoretical modeling in the Appendix and SI). So we have the relation of displacement and the stress as Fig. 2(B). The results revealed that the soft robot has excellent linear performance regardless of the actuation voltage level. With the flexible frame, the voltage-induced strain of DEA, that used to be nonlinear is transmitted to deploy the bending of arced frame, results in a quasi-linear displacement. Owing to the linear relation of the soft robot, we can direct input the open-circuit voltage from TENG to regulate the output motion of the soft robot, which help to reduces the complexity of the control system in the proposed TENG-Soft robot conjunction.

Supplementary material related to this article can be found online at doi:10.1016/j.nanoen.2021.106012.

Thanks to the construction of soft, compliant, and rigid material, the soft robot is of smoothing strain transmission from DEA to robotic body. This character rules out the auxiliary regulation and control scheme in the conventional soft robots. As a result, TENG can direct control and power the proposed soft robot through wire connections. The method of the measurement is described in SI as well. It is noteworthy that, when the applied voltage exceeds a threshold, wrinkles along the actuation direction were observed in the experiments, which are recorded in details in S6. wrinkles along the actuation direction were observed in the experiments, which are recorded in details in SI. The wrinkles induce out-of-plane deflections, which leads to electrical breakdown [42-44]. So, in the following section, we limit the voltage range to avoid wrinkles.

We first characterize the robot crawling locomotion with a conventional high voltage power source. The experimental setup is described in the SI. In Fig. 2(C), we show the speed of the robot subject to the alternating current (AC) voltages with different frequencies and voltage waveforms. The peak-to-peak voltage of 4 kV was prescribed, which is within the output range of the TENG. The speed peaks of 110 mm/s under a square wave voltage at 26 Hz, 51 mm/s under triangle wave at 28 Hz, and 69 mm/s under a sinusoidal wave at 30 Hz, respectively. The speed of the robot driven by a square wave is obviously higher than the other two groups, because the square wave signal has the maximum input energy. The robot reaches its maximum speed when the voltage frequency matches the natural frequency of the soft robot [17,29]. Based on the theoretical model, the natural frequency of the actuator can be expressed as Eq. (S1) and Fig. S5 in the SI, where a natural frequency of 28 Hz is identified. The duty cycle in square wave determines the loading and unloading time in one period. Fig. 2(D) describes the motion of the robot under several different duty cycles (time ratio of voltage on vs. the period). The speed of the robot achieves maximum speed at 50% duty cycle because the crawling motion is symmetric in the displacement of the fore and rear wheels, and the deformation of the DEA should be the same in the loading and unloading phases. Thus, a stable movement is attained. Fig. 2(E) measured the effect of voltage amplitude in the square waveform. As a parametric excitation, the high voltage will induce a higher order of resonance, over 100 Hz [45], which exceeds the frequency range of the dynamic voltage in TENG's output (about 15 Hz).

Fig. 2(F) and 2(G) shows the speeds of the robot under different payload weights. The frequency that corresponds to maximum speed is referred to as the optimized actuation frequency. As the payload increases, the optimized actuation frequency decreases since the natural frequency is shifted by a heavier loading. The experimental results confirm that the speed of the robot still reaches a maximum value of 15 mm/s under a 40 g payload, which is equivalent to about 4-fold of the robot weight. This is due to the change of the natural frequency of the soft robot, which is maximized deformed when the excitation frequency matches its natural frequency. A non-monotonic relation between the payload and speed is identified, which can be understood by considering the dynamics model of the soft robot (as analyzed in the SI). This result offers guidance for selecting the actuation frequency for a given payload mass and a targeting speed.

In Fig. 2(C)–(E), before reaching the peak speed, the soft robot exhibits a quasi-linear performance in the dynamic actuation, especially in the low-frequency range, which is well-suited for the operation of TENG. Also, in Fig. 2(F) and (G) before reaching the peak, the speed is linear with the payload weight. This linear behaviour is due to robotic design involving compliant and rigid materials instead of an entire soft robotic body.

In the above mechanical characterization of the soft robot, the applied actuation voltage level and frequency is attainable in the output value of TENG in a freestanding mode [37-39]. The static performance

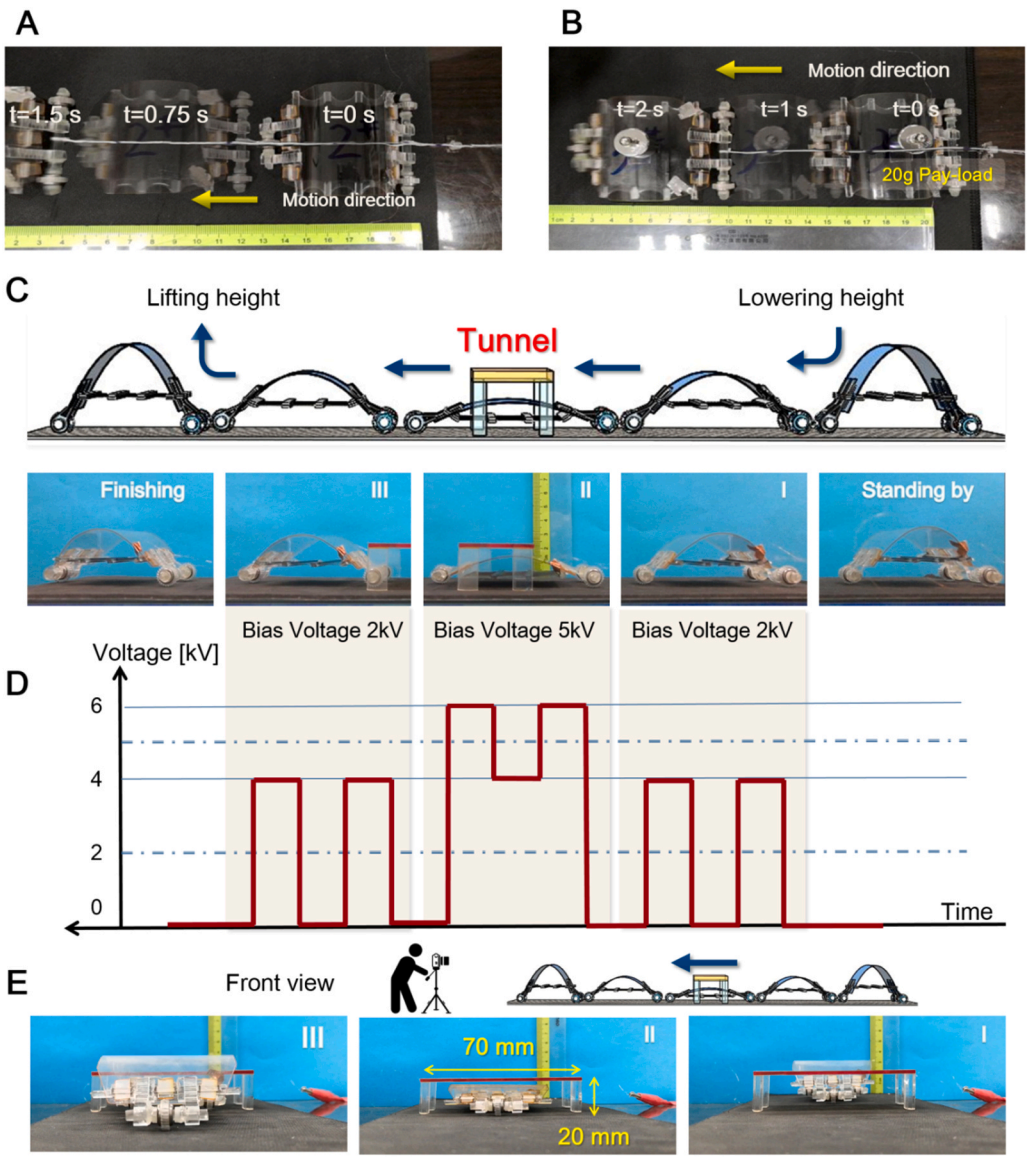

Fig. 3. Soft robot locomotion performance. (A) A series of snapshots of the soft robot motion at a frequency of 18 Hz. **(B)** The robot crawls at the speed of 50 mm/s with a payload of 20 g. **(C)** The soft robot passes a tunnel under an increased bias voltage level to lower its body. The left view of the robot moves through a narrow gap that is half the height of the robot. The process is composed of five states: standing by, I, II, III, and finishing. **(D)** State II, the bias voltage was raised, and the DEA vibrated at a new equilibrium state, which lowered the height of the robot. **(E)** The front view of the process when the robot is in action.

of TENG-driven DEA deformation has been modeled and verified [46]. Therefore, in the followings, we will focus on the robot locomotion characterization toward a direct TENG powering.

2.3. Soft robot crawling locomotion

Fig. 3(A) demonstrates the locomotion of the soft robot at the frequency of 18 Hz (the Supplementary Movie S2). Fig. 3(B) shows that the robot can move at the speed of 50 mm/s while carrying a payload of 20 g (the Supplementary Movie S3).

Supplementary material related to this article can be found online at doi:10.1016/j.nanoen.2021.106012.

In addition to passive bending of the robot under a payload, this soft robot features environmental adaptation by active body-arching. Fig. 3 (C) illustrates how the robot passes through a narrow tunnel (Width 70 mm × Length 30 mm × Height 20 mm) whose height is half of that of the robot. Fig. 3(D) provides the actuation strategy during the robot-travel. By lifting the bias voltage of the actuation voltage, a new equilibrium state, around which the DEA deforms dynamically, is attained. Then the height of the robot is lowered to adapt to the narrow gap. Fig. 3 (E) records the front view of this locomotion sequence (a video is provided as the Supplementary Movie S4). This offers a new perspective that, in a soft robot powered by two TENGs, where one TENG regulates the equilibrium state of the DEA to adjust the height of the soft robot meanwhile the other TENG controls robot's locomotion.

Supplementary material related to this article can be found online at doi:10.1016/j.nanoen.2021.106012.

2.4. TENG-Bot: powered and controlled by a freestanding TENG

Fig. 4 depicts the programmed sliding process of the TENG to power the soft robot and the generated voltage in the frequency domain, which was then measured by a high-voltage-probe with an attenuation. In the experimental setup, a motor drove the FEP in a reciprocating manner, and the sliding velocity was programmed by setting the accelerations in the motor. It ramps before reaching a plateau then declines. In Fig. 4(A)–(C), a programmed periodic motion is generated for the TENG sliding component. To measure the output voltage, the non-ground method was adopted [47], with a high voltage attenuation probe and the oscilloscope, which meets the standard of dielectric elastomer [48]. The output voltage of TENG is a complex periodic signal with different frequency components. It is then analyzed by Fast Fourier Transform (FFT) to identify the primary frequency, which can be applied to the theoretical model of the DEA-based soft robot, as in the method section. In the

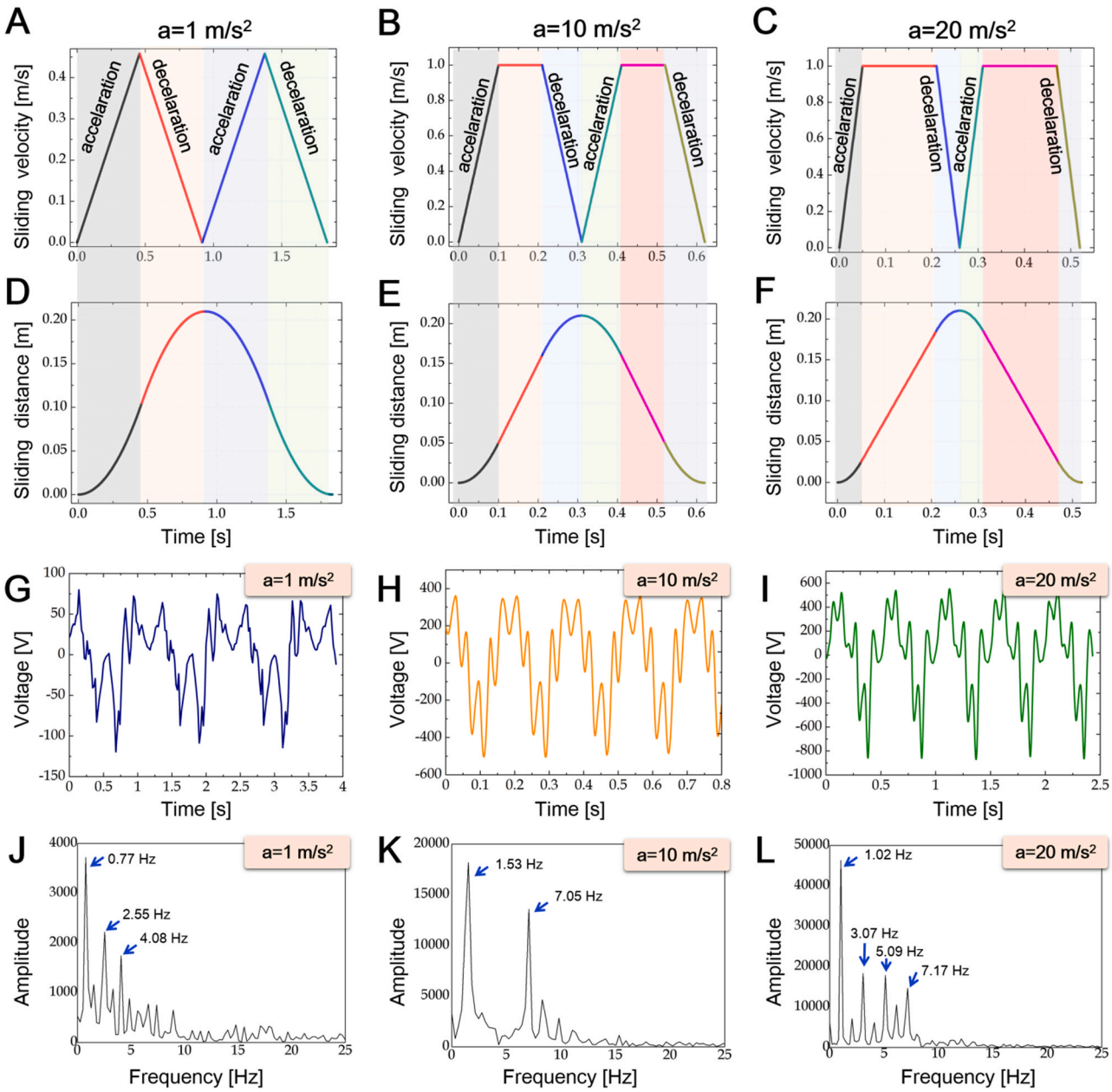

Fig. 4. The programmed sliding process and the generated electric energy in TENG. The mechanical energy is harvested by TENG and converted into periodic electric power. After a Fast Fourier Transform (FFT), the primary actuation frequency is identified. In the sliding of TENG, with an acceleration of a= 1 m/s^2, the sliding velocity is programmed in the form in **(A)**, and the sliding distance is in **(D)**. For a= 1, 10 and 20 m/s^2, the sliding velocity and the sliding velocity are in **(B)**, **(C)**, **(E)**, and **(F)**. The generated voltages in the time domain are plotted in **(G)–(I)**. The results of FFT are plotted in **(J)–(L)**, where each primary actuation frequency is identified.

freestanding TENG, the sliding distance is fixed, as related to Fig. 4(D)–(F), so that by setting the acceleration, we can program the sliding speed as in Fig. 4(A)–(C). Subject to the three acceleration, a = 1, 10, and 20 m/s^2, the generated voltages are different in the time domain and frequency range, in Fig. 4(G)–(L). The normalized amplitude illustrates the value of each primary frequency. In the current study, the harvested voltages by TENG are mainly limited at a low-frequency domain (< 10 Hz), which falls in the linear range of dynamic response of the soft robot. In Fig. 4(G)–(I), As the sliding acceleration of TENG increases, the driving voltage amplitude generated by friction increases significantly, while the displacement of TENG remains constant during the entire sliding process, so a larger sliding acceleration means a greater average speed. For soft robots under the same working conditions, when a greater voltage is applied, the larger the deformation in the DEA is attainable and the robot's speed is faster. In the experimental results (Fig. 4 G-I), it can be seen that as the acceleration of TENG increases, its open-circuit voltage also increases. The reason for the above phenomenon is that the great sliding acceleration of TENG promote the proportion of uniform motion in an motion cycle, thus results in a larger average speed of TENG. The more power and higher open-circuit voltage is generated. To further illustrate the characteristics of TENG, in the experiments, we also measured the output voltage by connecting the freestanding TENG with a ×1000 attenuator for the 6514 electrometers at the acceleration, a=1m/s^2. The data were real-time recorded and shown in Supplementary Figure S9. The open-circuit voltage and short-circuit transferred charges are basically in a stable amplitude range over time. Such results show that TENG can be used to drive soft robots excellently.

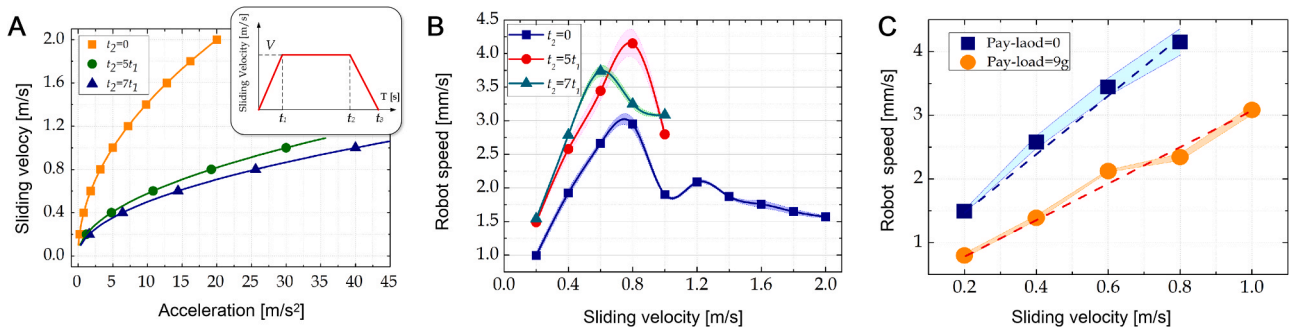

Fig. 5. The motion performance and the relation of the TENG-Bot. (A) The sliding velocity of the TENG in terms of different acceleration. **(B)** The speed of the soft robot controlled by the sliding velocity of the TENG.There is a monotonic relation when the TENG slides below 0.8 m/s. **(C)** The effect of the payload on the crawling speed control of a soft robot.

Fig. 5 presents the result of a TENG-Bot crawling by direct powering and control of TENG. In Fig. 5(A), the acceleration affects the average velocity of the TENG. This is due to the amount of accumulated electrical charges is related to the motion of sliding. With an abrupt change of the sliding velocity, more charges are generated, so the soft robot is powered further. Fig. 5(B) characterizes the relationship between the speed of the robot and the sliding velocity of the TENG which is direct correspondences, as a linear relation when the sliding speed is below 0.8 m/s. The soft robot with a payload capability of 9 g is achieved when driven by the freestanding mode TENG. In Fig. 5(C), an approximately linear relationship is attainable from the TENG motion to robotic motion. This offers the guidance of control and powering soft robot by harvesting the environmental dynamic motion via a potable TENG. Besides, the linear behavior of soft robot based on DEA is achieved, so that a simplified control strategy without an extra panel can benefit.

This results suggest a potential application that harvesting the vibration energy, which is used to be wasted, to actuate the motion of soft robot. In some dynamic mechanical systems, there are some parasitic vibration in low frequency range. To harvesting and storing the vibration as a new energy source has been proposed and investigated recently. In this paper, a TENG could not only effectively harvest the vibration energy but directly power a soft robot to crawl with a payload. This TENG-bot offers a new energy and control strategy for the DEA-based soft robot via a complimentary energy source from environmental vibration.

3. Conclusion

In this paper, we demonstrated a TENG-Bot for direct TENG power and control. A soft robot is proposed, consisting of a uni-directional DEA, a compliant arched robot body, and one-way bearing wheels. A theoretical model is established to characterize the electromechanical coupling of the DEA, which guided the design for the robot system that, for the first time, powered by Triboelectric Nanogenerator (TENG). In experimental characterization, we demonstrated that our soft robot is capable of locomotion with a speed of 110 mm/s (2.2 body length per second) under a square wave voltage of 4 kV at 26 Hz, and carry a maximum payload of 40 g (3.8 mass load ratio vs robot weight), which are superior to previously reported soft robots. Without additional actuators, this soft robot can adapt its morphology and pass through a narrow gap by merely adjusting the bias voltage.

Linear performance in both static and dynamic actuation schemes are achieved in the TENG-Bot which features a direct power-control by the freestanding mode TENG. The experimental results show an excellent linear relationship between the locomotion velocity of the soft robot and the sliding velocity of the TENG regardless of the payload, which has important guiding significance for the robot powering and control. The TENG-Bot proposed in this paper will pave a new way for the design of a new generation of smart soft robots for potable energy harvesting.

CRediT authorship contribution statement

W.S. designed and tested the actuator. B.L. analyzed results. F.Z. performed the soft robot experiments. C. F. performed the TENG experiments. X.G., C.C. and Y.L. discussed the results. G.C. C.Z. and Z.L.W. supervised the project. All the authors contributed to the writing of the manuscript.

Declaration of Competing Interest

The authors declare that they have no known competing financial interests or personal relationships that could have appeared to influence the work reported in this paper.

Acknowledgments

This work was supported by the National Key Research and Development Program of China (2019YFB1311600), Natural Science Foundation of China (Grant No. 11902248, 52075411 and 91748124), Shaanxi Key Research and Development Program (2020ZDLGY06-11), and the State Key Laboratory for Strength and Vibration of Mechanical Structures (SV2018-KF-08).

Appendix A

The experimental setup for the DE actuator (DEA)

During the test, the signal generator (RIGOL DG1032Z) and the high-voltage amplifier (TREK 610E) are used as the drive equipment for the DEA. A laser displacement sensor (Panasonic IEC60825-1) is used to record the length change of the DEA. A force sensor (LANRIN AUMI) is used to record the blocking force of the DEA with voltage. A 12Bit-ADC (NI cRIO-9035) converts the analog signals collected by the laser displacement sensor and the force sensor into digital signals to the computer. The experimental setup is illustrated in Figure S7.

Displacement characterization. When measuring the relationship between displacement and voltage, we fixed one end of the DEA so that the other end could slide freely. (1) Installing an L-shaped cardboard on the free end of the DEA to make the laser beam shine on the cardboard; (2) Applying voltage to the DEA through the signal generator and high-voltage amplifier; (3) Recording the data until the DE film broke down; (4) Converting the

analog signal collected by the laser displacement sensor into a digital signal during the test and then sending it to the computer for processing; (5) 5 samples were measured for different pre-stretching and taking the average value after completion.

Impedance blocking force and voltage. To measure the impedance blocking force, we fixed one end of the DE actuator on the bracket and placed the other end in contact on the force sensor platform. The specific operation steps are as follows: (1) In the initial state, the free end of the DEA and the force sensor were in a critical contact state, and the force sensor reading should be zero at this time; (2) Applying voltage to the DEA through the signal generator and high-voltage amplifier; (3) Recording the data until the DE film broke down; (4) Collecting the analog signal in the force sensor and converting it to the computer for processing; (5) 5 samples were tested and taking the average value.

The experimental setup for the soft robot crawling

The average speed is used to characterize the robot locomotion performance. (1) Connecting a string of no mass to the tail of the robot, and marking the positions of 0mm, 50mm, 100mm, and 150mm respectively; (2) Passing the string through the fixed mark points before the test, and fix the 0 position and overlapping to the 0mm; (3) While the robot is powered, using a stopwatch to record the time as robot travel through the marked points; (4) Calculating the corresponding speed when the robot moves 50mm, 100mm, 150mm respectively. Take the average value as the movement speed of this test; (5) Testing at least 3 samples in each group with repeat 5 times for each sample, and taking the final average value as the movement speed value of the robot; (6) In order to avoid the breakdown in DE film, the peak-to-peak voltage applied to the robot during the experiment is limited within 4kV. In addition, rest 30 s as the interval of each group of experiments. The experimental setup is sketched in Figure S8.

Measurement of TENG output

A oscilloscope and a high voltage robe are used to measure the output properties of the TENG. The specific operation process can be described as follows: (1) The two copper electrodes of the TENG were connected via the wires to the high-voltage probe (Tektronix P6015A); (2) The attenuated voltage output was recorded by the high-voltage probe to the oscilloscope, and then record as the output characteristics of TENG in different sliding modes through the oscilloscope (as shown in Fig. 4 A-F); (3) The collected data was processed to analyze the TENG output response corresponding to the three different motion modes, as shown in Fig. 4 G-I.

The electromechanical coupling model in the DEA

Targeting on the TENG-powering, we establish a model to estimate the performance of the DEA based on the Euler-Lagrange method [49,50]. Most of DE materials are commonly regarded as a typical viscoelastic material, primarily when the VHB film is employed. Therefore, it is essential to take the influence of viscoelasticity into account in the modeling [51,52].

Fig. 2(A) shows the simplified sketch of geometrical parameters. In the pre-stretched state, because of the constraints in the frame, the bending angle of the frame is θ_0, the length of the DEA is $\lambda_{1p}L_1$, and the length of the frame is c. The width of the DEA is fixed by the PMMA bar at $\lambda_{2p}L_2$. In the actuated state, the DEA is subjected to the voltage Φ, the wide stretch is assumed to be fixed by the bars $\lambda_2 = \lambda_{2p}$, but the long-stretch λ_1 is a function of actuation displacement ΔL, and is calculated as $\lambda_1 = \Delta L L_1/\lambda_{1p} + 1$. The stretches λ_i (i = 1,2,3) is denoted in Fig. S2 of SI.

The total potential energy of the actuator is a summation of the potential energy of the DE DEA and the frame. Considering the flexible frame has a constant bending moment along with the frame, we write its potential energy as a function of the bending angle [53–55]:

$$U_F = \frac{1}{2}K_b\theta^2 \tag{1}$$

where K_b is the bending stiffness, and the θ is the bending angle of the frame.

To use the Euler Lagrange method, we need to calculate the kinetic energy of the system. Due to the weights of the DE membrane and the constraint fibers are smaller than the frame, by considering the frame as a rotational joint, the kinetic energy of the system has the form:

$$E_F = \frac{1}{2}J\dot{\theta}^2 \tag{2}$$

in which J denote the polar moment of the frame.

In the pure shear model, boundary conditions$\lambda_2 = \lambda_{2p}$can be achieved [53]. The curved length of the frame c is linked to the DE membrane length $\lambda_1 L_1$ by the bending angle of the frame θ, so that λ_1 can be expressed as a function of the θ. We set inelastic stretches as $\xi_1 = \xi$ and defined the Lagrangian of the system as $L(\theta, \dot{\theta}, \xi, \overline{E}) = E_F(\dot{\theta}) - U_F(\theta) - U_{DE}(\theta, \xi, \overline{E})$ with the nominal electrical field $\overline{E} = \Phi/H$. The Euler-Lagrange equation for the non-conservative systems is given by:

$$\frac{d}{dt}\left(\frac{\partial L}{\partial \dot{q}_i}\right) - \frac{\partial L}{\partial q_i} + \frac{\partial D}{\partial \dot{q}_i = 0, i=1,2} \tag{3}$$

with D the dissipation function, q_i is the independent generalized coordinates. $q_1 = \theta$ describes the bending deformation, and $q_2 = \xi$ characterizes the stretch of the dashpot in the viscoelastic model (Fig. S4). For ease of calculation, we use the Rayleigh dissipation function for a Newtonian fluid dashpot in the following context:

$$D = \frac{1}{2}\eta\dot{\xi}^2 Vol \tag{4}$$

in which η corresponds to the viscosity of the dashpot.

Inserting (1), (2), (4) and (S2) into Eq. (3) lead to a system of two ordinary nonlinear differential equations:

$$\frac{d^2\theta}{dt^2} + g\left(\theta, \xi, \Phi, \lambda_{1p}, \lambda_{2p}\right) = 0$$

$$g = \frac{Vol}{J}\left[\mu_\alpha\left(\lambda - \lambda^{-3}\lambda_{2p}^{-2}\right) + \mu_\beta\left(\lambda\xi^{-2} - \lambda^{-3}\xi^2\right) - \frac{\varepsilon\Phi^2}{H^2}\lambda\lambda_{2p}^2\right]\frac{2c\lambda_{1p}}{L_{1p}}\left(-\theta^{-2}\sin\frac{\theta}{2} + \frac{1}{2\theta}\cos\frac{\theta}{2}\right) + \frac{K_b\theta}{J} \tag{5}$$

$$\frac{d\xi}{dt} = \frac{\mu_\beta}{\eta}\left(\lambda^2\xi^{-3} - \lambda^{-2}\xi\right) \tag{6}$$

Eqs. (5) and (6) constitute the core of the governing equations for the DEA. From Eq. (5) we obtained the equilibrium state of the DEA :

$$Vol\left[\mu_\alpha\left(\lambda - \lambda^{-3}\lambda_{2p}^{-2}\right) - \frac{\varepsilon\Phi^2}{H^2}\lambda\lambda_{2p}^2\right]\frac{2c\lambda_{1p}}{L_{1p}}\left(-\theta^{-2}\sin\frac{\theta}{2} + \frac{1}{2\theta}\cos\frac{\theta}{2}\right) + K_b\theta = 0$$

$$\lambda = \frac{2c\lambda_{1p}}{L_{1p}}\frac{1}{\theta}\sin\frac{\theta}{2} \tag{7}$$

In the static actuation, the elastic stress in DEA is always in equilibrium with the tensile force of the frame, so that the blocking force is expressed as

$$F_B = \frac{\varepsilon\Phi^2}{H^2}\lambda_{1p}^2\lambda_{2p}^2 \times \frac{Vol}{L_{1p}} \tag{8}$$

Appendix B. Supporting information

Supplementary data associated with this article can be found in the online version at doi:10.1016/j.nanoen.2021.106012.

References

[1] D. Rus, M.T. Tolley, Design, fabrication and control of soft robots, Nature 521 (2015) 467–475.
[2] C. Laschi, B. Mazzolai, M. Cianchetti, Soft robotics: Technologies and systems pushing the boundaries of robot abilities, Sci. Robot. 1 (2016) eaah3690.
[3] W. Hu, G.Z. Lum, M. Mastrangeli, M. Sitti, Small-scale soft-bodied robot with multimodal locomotion, Nature 554 (2018) 81–85.
[4] T.G. Thuruthel, B. Shih, C. Laschi, M.T. Tolley, Soft robot perception using embedded soft sensors and recurrent neural networks, Sci. Robot. 4 (2019) eaav1488.
[5] S.I. Rich, R.J. Wood, C. Majidi, Untethered soft robotics, Nat. Electron. 1 (2018) 102–112.
[6] M. Sitti, Miniature soft robots—road to the clinic, Nat. Rev. Mater. 3 (2018) 74.
[7] S. Kurumaya, B.T. Phillips, K.P. Becker, M.H. Rosen, D.F. Gruber, K.C. Galloway, K. Suzumori, R.J. Wood, A Modular Soft Robotic Wrist for Underwater Manipulation, Soft robot (2018) 5399–5409.
[8] C. Walsh, Human-in-the-loop development of soft wearable robots, Nat. Rev. Mater. 3 (2018) 78–80.
[9] Y. Qiu, E. Zhang, R. Plamthottam, Q. Pei, Acc. Dielectric Elastomer Artificial Muscle: Materials Innovations and Device Explorations, Chem. Res. 52 (2019) 316–325.
[10] C. Cao, X. Gao, A.T. Conn, A compliantly coupled dielectric elastomer actuator using magnetic repulsion, Appl. Phys. Lett. 114 (2019), 011904.
[11] C. Cao, L. Chen, W. Duan, T.L. Hill, B. Li, G. Chen, Y. Li, L. Wang, X. Gao, On the mechanical power output comparisons of cone dielectric elastomer actuators, IEEE/ASME Trans, Mechatronics. (2021).
[12] X. Gao, C. Cao, J. Guo, A.T. Conn, Elastic Electroadhesion with Rapid Release by Integrated Resonant Vibration, Adv. Mater. Technol. 4 (2019) 1800378.
[13] G. Gu, J. Zou, R. Zhao, X. Zhao, X. Zhu, Soft wall-climbing robots, Sci. Robot. 3 (2018) eaat2874.
[14] C. Christianson, N.N. Goldberg, D.D. Deheyn, S. Cai, M.T. Tolley, Translucent soft robots driven by frameless fluid electrode dielectric elastomer actuators, Sci. Robot. 3 (2018) eaat1893.
[15] T. Li, G. Li, Y. Liang, T. Cheng, J. Dai, X. Yang, B. Liu, Z. Zeng, Z. Huang, Y. Luo, T. Xie, W. Yang, Fast-moving soft electronic fish, Sci. Adv. 3 (2017), e1602045.
[16] C. Tang, W. Ma, B. Li, M. Jin, H. Chen, Cephalopod-Inspired Swimming Robot Using Dielectric Elastomer Synthetic Jet Actuator, Adv. Eng. Mater. 22 (2020) 1901130.
[17] C. Tang, B. Li, H. Fang, Z. Li, H. Chen, A speedy, amphibian, robotic cube: Resonance actuation by a dielectric elastomer, Sensor. Actuat. A-Phys. 270 (2018) 1–7.
[18] W.B. Li, W.M. Zhang, H.X. Zou, Z.K. Peng, G. Meng, A. Fast, Rolling Soft Robot Driven by Dielectric Elastomer, IEEE/ASME Trans. Mechatron 23 (2018) 1630–1640.
[19] E.F.M. Henke, S. Schlatter, I.A. Anderson, Soft Dielectric Elastomer Oscillators Driving Bioinspired Robots, Soft Robot 4 (2017) 353–366.
[20] W. Sun, F. Liu, Z. Ma, C. Li, J. Zhou, Soft mobile robots driven by foldable dielectric elastomer actuators, J. Appl. Phys. 120 (2016), 084901.
[21] X. Ji, X. Liu, V. Cacucciolo, M. Imboden, Y. Civet, A.E. Haitami, S. Cantin, Y. Perriard, H. Shea, An autonomous untethered fast soft robotic insect driven by low-voltage dielectric elastomer actuators, Sci. Robot. 4 (2019) eaaz6451.
[22] X. Yang, L. Chang, N.O. Pérez-Arancibia, An 88-milligram insect-scale autonomous crawling robot driven by a catalytic artificial muscle, Sci. Robot. 5 (45) (2020) eaba0015.
[23] S. Shian, K. Bertoldi, D.R. Clarke, Dielectric Elastomer Based "Grippers" for Soft Robotics, Adv. Mater. 27 (2015) 6814–6819.
[24] J. Shintake, S. Rosset, B. Schubert, D. Floreano, H. Shea, Versatile Soft Grippers with Intrinsic Electroadhesion Based on Multifunctional Polymer Actuators, Adv. Mater. 28 (2016) 231–238.
[25] C. Cao, X. Gao, A.T. Conn, Soft Robotics: A Magnetically Coupled Dielectric Elastomer Pump for Soft Robotics, Adv. Mater. Technol. 4 (2019) 1900128.
[26] Y. Chen, H. Zhao, J. Mao, P. Chirarattananon, E.F. Helbling, N.P. Hyun, D. R. Clarke, R.J. Wood, Controlled flight of a microrobot powered by soft artificial muscles, Nature 575 (2019) 324–329.
[27] S. Schlatter, P. Illenberger, S. Rosset, Peta-pico-Voltron: An open-source high voltage power supply, Peta-pico-voltron: HardwareX 4 (2018), e00039.
[28] H. Zhao, A.M. Hussain, M. Duduta, D.M. Vogt, R.J. Wood, D.R. Clarke, Compact Dielectric Elastomer Linear Actuators, Adv. Funct. Mater. 28 (2018) 1804328.
[29] T. Yang, Y. Xiao, Z. Zhang, Y. Liang, G. Li, M. Zhang, S. Li, T.W. Wong, Y. Wang, T. Li, Z. Huang, A soft artificial muscle driven robot with reinforcement learning, Sci. Rep. 8 (2018) 1–8.
[30] C. Zhang, W. Tang, Y.K. Pang, C.B. Han, Z.L. Wang, Active Micro-Actuators for Optical Modulation Based on a Planar Sliding Triboelectric Nanogenerator, Adv. Mater. 27 (2015) 719–726.
[31] Z.L. Wang, On Maxwell's, displacement current for energy and sensors: the origin of nanogenerators, Mater. Today 20 (2017) 74–82.
[32] J. Zhao, G. Zhen, G. Liu, T. Bu, W. Liu, X. Fu, P. Zhang, C. Zhang, Z.L. Wang, Remarkable merits of triboelectric nanogenerator than electromagnetic generator for harvesting small-amplitude mechanical energy, Nano Energy 61 (2019) 111–118.
[33] H.F. Qin, G.Q. Gu, W.Y. Shang, H.C. Luo, W.H. Zhang, P. Cui, B. Zhang, J.M. Guo, G. Cheng, Z.L. Du, Bulk Pt/CsPbBr 3 Schottky junctions for charge boosting in robust triboelectric nanogenerators, Nano Energy 68 (2020), 104372.
[34] H.F. Qin, G. Cheng, Y.L. Zi, G.Q. Gu, B. Zhang, W.Y. Shang, F. Yang, J.J. Yang, Z. L. Du, Z.L. Wang, High energy storage efficiency triboelectric nanogenerators with unidirectional switches and passive power management circuits, Adv. Funct. Mater. 28 (2018) 1805216.
[35] C. Zhang, W. Tang, C. Han, F. Fan, Z.L. Wang, Theoretical comparison, equivalent transformation, and conjunction operations of electromagnetic induction generator and triboelectric nanogenerator for harvesting mechanical energy, Adv. Mater. 26 (2014) 3580–3591.
[36] G.Z. Yang, J. Bellingham, P.E. Dupont, P. Fischer, L. Floridi, R. Full, N. Jacobstein, V. Kumar, M. McNutt, R. Merrifield, B.J. Nelson, B. Scassellati, M. Taddeo, R. Taylor, M. Veloso, Z.L. Wang, R. Wood, The grand challenges of Science Robotics, Sci. Robot. 3 (2018) eaar7650.
[37] X. Chen, Y. Wu, A. Yu, L. Xu, L. Zheng, Y. Liu, H. Li, Z.L. Wang, Self-powered modulation of elastomeric optical grating by using triboelectric nanogenerator, Nano Energy 38 (2017) 91–100.

[38] X. Chen, X. Pu, T. Jiang, A. Yu, L. Xu, Z.L. Wang, Tunable Optical Modulator by Coupling a Triboelectric Nanogenerator and a Dielectric Elastomer, Adv. Funct. Mater. 27 (2017) 1603788.
[39] Y. Xie, S. Wang, S. Niu, L. Lin, Q. Jing, J. Yang, Z. Wu, Z.L. Wang, Grating-Structured Freestanding Triboelectric-Layer Nanogenerator for Harvesting Mechanical Energy at 85% Total Conversion Efficiency, Adv. Mater. 26 (2014) 6599–6607.
[40] H. Fang, W. Wu, J. Song, Z.L. Wang, Controlled growth of aligned polymer nanowires, J. Phys. Chem. C 113 (2009) 16571–16574.
[41] W. Wang, Y. Wang, K. Wang, H. Zhang, J. Zhang, Analysis of the kinematics of module climbing caterpillar robots, IEEE/ASME Adv. Int. Mech (2008) 84–89.
[42] J. Zhu, M. Kollosche, T. Lu, G. Koford, Z. Suo, Two types of transitions to wrinkles in dielectric elastomers, Soft Matter 8 (2012) 8840–8846.
[43] H. Godaba, Z.Q. Zhang, U. Gupta, C.C. Foo, J. Zhu, Dynamic pattern of wrinkles in a dielectric elastomer, Soft matter 13 (2017) 2942–2951.
[44] L. Shui, Y. Liu, B. Li, C. Zou, C. Tang, L. Zhu, X. Chen, Mechanisms of electromechanical wrinkling for highly stretched substrate-free dielectric elastic membrane, J. Mech. Phys. Solids 122 (2019) 520–537.
[45] C. Tang, B. Li, L. Liu, S.S. Ge, L. Shui, H. Chen, Nonlinear out-of-plane resonation of a circular dielectric elastomer, Smart Mater. Struct. 29 (2020), 045003.
[46] X. Chen, T. Jiang, Z.L. Wang, Modeling a dielectric elastomer as driven by triboelectric nanogenerator, Appl. Phys. Lett. 110 (2017), 033505.
[47] W.H. Zhang, G.Q. Gu, H.F. Qin, S.M. Li, W.Y. Shang, T.Y. Wang, B. Zhang, P. Cui, J. M. Guo, F. Yang, G. Cheng, Z.L. Du, Measuring the actual voltage of a triboelectric nanogenerator using the non-grounded method, Nano Energy 77 (2020), 105108.
[48] F. Carpi, I. Anderson, S. Bauer, G. Frediani, G. Gallone, M. Gei, C. Graaf, C. Jean-Mistral, W. Kaal, G. Kofod, Standards for dielectric elastomer transducers, Smart Mater. Struct. 24 (2015), 105025.
[49] B.X. Xu, R. Mueller, Dynamic analysis of dielectric elastomer actuators, Appl. Phys. Lett. 100 (2012), 112903.
[50] D. Eder-Goy, Y. Zhao, B.X. Xu, Dynamic pull-in instability of a prestretched viscous dielectric elastomer under electric loading, Acta Mech 228 (2017) 4293–4307.
[51] C.C. Foo, S. Cai, S.J.A. Koh, S. Bauer, Z. Suo, Model of dissipative dielectric elastomers, J. Appl. Phys. 111 (2012), 034102.
[52] W. Hong, Modeling viscoelastic dielectrics, J. Mech. Phys. Solids 59 (2011) 637–650.
[53] H. Vatanjou, Y. Hojjat, M. Karafi, Nonlinear dynamic analysis of dielectric elastomer minimum energy structures, Appl. Phys. A Mater. Sci. Process. 125 (2019) 1–11.
[54] J. Zou, G. Gu, Dynamic modeling of dielectric elastomer actuators with a minimum energy structure, Smart Mater. Struct. 28 (2019), 085039.
[55] F. Liu, J. Zhou, Shooting and arc-length continuation method for periodic solution and bifurcation of nonlinear oscillation of viscoelastic dielectric elastomers, J. Appl. Mech. 85 (2018), 011005.

Wenjie Sun received the Ph.D. degree in solid mechanics from Xi'an Jiao tong University in 2016. He joined Xi'an University of Technology in 2017 and is currently lecturer of the school of mechanical and precision instrument engineering. His research interests include soft robotics, mechanics of soft materials, and structural mechanics.

Bo Li was awarded his Ph.D. degree in instrumental science and technology from Xi'an Jiaotong University, Xi'an, China, in 2012. He is currently an associate professor at Xi'an Jiaotong University. He is the Associate Editor for IEEE Transaction on Automation Sciences and Engineering.

Fei Zhang received his B.S.degree in mechanical design manufacture and automation from the Suzhou University in 2016. He was awarded the master's degree in mechanical engineering from Xi'an University of Technology in 2020. His research interests are mainly focused on dielectric elastomer and soft robot.

Chunlong Fang received his B.S. degree in material chemistry from the Shaanxi Normal University in 2017. He received master's degree under the supervision of Professor Chi Zhang at the University of Chinese Academy of Sciences in 2020. His research interests are mainly focused on tribotronics and self-powered microactuators.

Yanjun Lu was awarded his Ph.D. degree in Mechatronics Engineering from Xi'an Jiaotong University, Xi'an, China, in 2005. He is now a professor at Xi'an University of Technology. His research interests include tribology, intelligent manufacturing, lubrication theroy, mechanical dynamics and reliability.

Xing Gao received his M.Sc. and Ph.D. degrees in mechanical engineering from Loughborough University, UK in 2012 and 2016, respectively. He is currently an Associate Professor at Research Centre for Medical Robotics and Minimally Invasive Surgical Devices, Shenzhen Institute of Advanced Technology, Chinese Academy of Sciences. His research interests include smart materials, intelligent structures and soft robotics.

Chongjing Cao was awarded the Ph.D. in robotics and autonomous systems from University of Bristol, UK, in 2019. He is now with the Shenzhen Institute of Advanced Technology, Chinese Academy of Sciences where he is a postdoc researcher. His research interests include bio-inspired robotic systems and the dynamics of soft actuators.

Guimin Chen received B.S., M.S., Ph.D. from the School of Mechatronics Engineering of Xidian University in 2000, 2003 and 2005. He is now a full professor at Xi'an Jiaotong University and the dean of institute of intelligent robots. He is the Associate Editor of ASME Journal of Mechanisms and Robotics.

Prof. Chi Zhang received his Ph.D. degree from Tsinghua University in 2009. After graduation, he worked at Tsinghua University as a postdoc research fellow and NSKLtd., Japan as a visiting scholar. He now is the principal investigator of Tribotronics Group in Beijing Institute of Nanoenergy and Nanosystems, Chinese Academy of Sciences (CAS). Prof. Chi Zhang's research interests are triboelectric nanogenerator, tribotronics, self-powered MEMS/NEMS, and applications in flexible electronics, intelligent equipment and the Internet of things. He has been awarded by National Natural Science Foundation of China for Excellent Young Scientist Award.

Prof. Zhong Lin Wang received his Ph.D. from Arizona State University in physics. He now is the Hightower Chair in Materials Science and Engineering, Regents' Professor, Engineering Distinguished Professor and Director, Center for Nanostructure Characterization, at Georgia Tech. Dr. Wang has made original and innovative contributions to the synthesis, discovery, characterization and understanding of fundamental physical properties of oxide nanobelts and nanowires, as well as applications of nanowires in energy sciences, electronics, optoelectronics and biological science. His discovery and breakthroughs in developing nanogenerators established the principle and technological road map for harvesting mechanical energy from environment and biological systems for powering personal electronics. His research on self-powered nanosystems has inspired the worldwide effort in academia and industry for studying energy for micro-nano-systems, which is now a distinct disciplinary in energy research and future sensor networks. He coined and pioneered the field of piezotronics and piezophototronics by introducing piezoelectric potential gated charge transport process in fabricating new electronic and optoelectronic devices. Details can be found at: http://www.nanoscience.gatech.edu.